Waterborne, Semicrystalline, Pressure-Sensitive Adhesives with Temperature-Responsiveness and Optimum Properties

Amaia Agirre,[†] Carolina de las Heras-Alarcón,[‡] Tao Wang,[‡] Joseph L. Keddie,[‡] and José M. Asua*[,†]

Institute of Polymer Materials (POLYMAT) and Grupo de Ingeniería Química, Edificio Korta I+D+I, The University of the Basque Country, 20018 Donostia-San Sebastián, Spain, and Department of Physics and Surrey Materials Institute, University of Surrey, Guildford GU2 7XH, United Kingdom

ABSTRACT The synthesis and resulting temperature-responsive properties of semicrystalline waterborne pressure-sensitive adhesives (PSAs) were investigated. A crystalline polymer fraction was produced in situ within waterborne particles by miniemulsion polymerization of non-branched long chain acrylates. The degree of crystallinity was controlled by copolymerization with a short chain acrylate. The polymerization strategy determined the polymer architecture and film structure, which then influenced the adhesion properties. The high sensitivity of the adhesion strength of these PSAs to temperature, in the range around the crystal melting point, opens up the possibility of designing temperature-responsive adhesives. With the right distribution and concentration of crystalline polymers, a simultaneous increase in both the peel strength and the shear resistance was obtained, which is a combination that is often not found when optimizing adhesive properties.

KEYWORDS: miniemulsion polymerization • temperature-responsive • pressure-sensitive adhesives • crystallinity • stearyl acrylate • adhesion properties • shear • peel strength.

INTRODUCTION

Pressure-sensitive adhesives (PSA) are viscoelastic materials that can adhere strongly to solid surfaces upon application of light contact pressures and short contact times. PSAs are commonly applied as a polymeric thin layer on a substrate and can be a part of products ranging from simple applications, such as self-adhesive envelopes and self-adhesives stamps, to highly sophisticated ones, such as in the automotive, aerospace, and electronic industries (1−8). Considering their nature, they are classified as: hot-melt, solventborne, and waterborne. Waterborne PSAs are advantageous as they do not need any heating (unlike the hot melt adhesives) and are more environmentally friendly than the solventborne PSAs, because they do not emit volatile organic compounds during their film formation.

Among the different base polymers used for waterborne PSAs, acrylates have enjoyed the fastest growth in commercial applications. Their popularity is attributable to optical clarity, UV light and oxidation stability, low toxicity, and relatively low cost. Polymers formed from short chain acrylates are completely amorphous and their adhesion performance is determined by the polymer architecture, such as cross-link density, molecular weight distribution, and branching (9).

In the case of thermoplastic polymers (ethylene vinyl acetate (EVA)/aromatic hydrocarbon resin blends (10), hot melt polyurethanes (PUs) (11), polypropylene-polyamide 6 (PP-PA6) systems (12, 13), and structured fluorinated polymers (14)), it has been reported that the presence of a crystalline fraction can have profound effects on the adhesion properties. Polymers with crystallizable side chains have been used as PSAs in which the adhesion can be switched on/off by changing the temperature (15). These materials exhibit a sharply defined melting temperature, above which the adhesion drops strongly. Temperature-switchable PSAs have medical applications (e.g., in bandages for fragile skin) (16) and would be useful for recycling parts that are adhered together. An important drawback of these materials is that they are either hot melt or solvent-borne adhesives, and therefore they cannot benefit from the advantages of waterborne systems. On the other hand, there is a challenge in developing waterborne PSAs to achieve an optimum in both the peel strength and the shear holding power, as will be discussed further in this paper.

In this work, waterborne, semicrystalline pressure sensitive adhesives were developed. The crystalline fraction of the polymer was produced in situ by miniemulsion polymerization of non-branched long chain acrylates. The degree of crystallinity was controlled by copolymerization with a short chain acrylate.

* Corersponding author. E-mail: jm.asua@ehu.es.
Received for review October 13, 2009 and accepted January 5, 2010
[†] The University of the Basque Country.
[‡] University of Surrey.
DOI: 10.1021/am9006947

Table 1. Summary of the Compositions of the Latexes Synthesized

	monomer composition		
latex	SA (wt %)	2EHA (wt %)	MAA (wt %)
Latex 1	3.85	94.23	1.92
Latex 2	80	19.6	0.4
Latex SA100	100		
Latex SA80	79.81	19.64	0.55
Latex SA60	60.63	38.47	0.9
Latex SA40	41.52	57.25	1.23
Latex SA20	22.69	76.15	1.16

Polymers formed by long-chain acrylates (chain length greater than 9−10 carbons) are able to crystallize through ordering of their side chains. Unlike the situation for conventional semicrystalline polymers in which the backbone crystallizes, crystallinity is provided by the long *n*-alkyl side chain of the polymer. Octadecyl acrylate (commercially known as stearyl acrylate, SA) was used in this work. Copolymerization of non-branched long chain acrylates with short chain acrylates, which decrease the degree of crystallinity of the polymer, has been used elsewhere to control the degree of crystallinity (17−19). 2-Ethylhexyl acrylate was used in this work. Because SA is a hydrophobic monomer that barely diffuses through the aqueous phase, conventional emulsion polymerization is not suitable to synthesize the copolymer unless a phase transfer agent such as cyclodextrin (20, 21) is used. Therefore, miniemulsion polymerization (22, 23) was used. The use of SA is very convenient because it plays the role of the costabilizer during the miniemulsification, and hence there is no need for using a non-reactive costabilizer, such as hexadecane. The effect of the polymerization strategy on the polymer architecture and the consequent effects on the adhesion properties were investigated.

EXPERIMENTAL SECTION

Materials. 2-Ethylhexyl acrylate (2EHA) (Quimidroga), methacrylic acid (MAA) (Aldrich), and octadecyl acrylate (stearyl acrylate, SA, Aldrich) were used as received. Alkyldiphenyloxide disulfonate (Dowfax 2A-1, Dow Chemical Company) was used as anionic emulsifier. Ammonium persulfate (FLUKA Chemika) was used as an initiator. THF (99.9% GPC, Scharlab) was used as a solvent.

Experimental Design. The latexes synthesized are summarized in Table 1. All of them were prepared by miniemulsion polymerization. The number following SA in the name of the latexes represents the nominal weight percent concentration of SA. Latex 1 is a regular amorphous PSA polymer, which was used as a reference, as well as one of the components of the latex blends (see Table 2). For a given SA/2EHA monomer ratio, the maximum degree of crystallinity is expected when all of SA is polymerized first and the 2EHA is polymerized afterwards, and vice versa. This strategy is likely to result in phase separation between the poly(SA) and the poly(2EHA). A certain amount of compatibilizing poly(SA-co-2EHA) is expected to reduce phase separation. Therefore, in this work, the complex poly(SA)/poly(SA-co-2EHA)/poly(2EHA) latex was mimicked by blending in different proportions Latex 1, which is mainly constituted of 2EHA, and Latex 2, which is a semicrystalline poly(SA)/poly(SA-co-2EHA) latex (Table 2). Latex 2 was produced by homopolymerizing first a large fraction of the SA and then copolymerizing the rest of the SA with 2EHA and MAA. Latex SA100 was synthesized by homopolymerizing SA. It was used as a reference for DSC measurements.

Table 2. Summary of the Components and the Monomer Compositions of the Latex Blends

			monomer composition		
blend	Latex 1 (wt %)	Latex 2 (wt %)	SA (wt %)	2-EHA (wt %)	MAA (wt %)
Blend SA60	25	75	60.96	38.26	0.78
Blend SA40	50	50	41.92	56.92	1.16
Blend SA20	75	25	22.89	75.57	1.54

Table 3. Formulations Used to Prepare Latex 1 and 2

	amount (g)	
ingredient	Latex 1	Latex 2
water	394.07	394.16
2-ethylhexyl acrylate (2-EHA)	367.52	75.3
methacrylic acid (MAA)	7.75	1.5
stearyl acrylate (SA)	15	299.99
Dowfax 2A-1	8.52	8.3
$(NH_4)_2S_2O_8$	1.99	1.89

For each SA/2EHA monomer ratio, the minimum degree of crystallinity is expected when SA and 2EHA are copolymerized together, because the incorporation of short chain acrylates reduces the degree of crystallization. In order to assess the performance of latexes with lower degrees of crystallinity, latexes SA80 through SA20, which had decreasing SA contents varying from 80 wt % (SA80) to 20 wt % (SA20), were produced in batch miniemulsion copolymerization of SA and 2EHA. The crystallinity was expected to decrease from Latex SA80 to SA20. The overall compositions of these latexes were the same as those of Latex 2 and the blends.

Preparation of the Miniemulsions. Miniemulsions were prepared as follows. Dowfax 2A-1, water and the monomers were mixed. Because of the low water solubility of SA and its physical characteristics (solid form), it was necessary to ultrasonify the mixture to obtain an emulsion. This coarse emulsion was sonified with a Branson Sonifier (amplitude 80 and energy pulsed at 1 Hz) over 10 min in an ice bath to avoid overheating.

Miniemulsion Polymerizations. Latex 1 was prepared batchwise using the formulation shown in Table 3 in a 750 mL jacketed glass reactor fitted with a reflux condenser, a sampling device, N_2 inlet, and a stainless steel impeller rotation at 200 rpm. The reaction was carried out at 70 °C for 2 h.

Latex 2 was prepared by first homopolymerizing a substantial part of SA and then copolymerizing the rest of the SA with 2-EHA and MAA. The goal was to homopolymerize 60 wt % SA, adding then the mixture of 2-EHA and MAA. In practice, this requires a fast and reliable method to monitor the conversion of SA. Reaction calorimetry meets these requirements (24). Therefore, in order to estimate the heat of polymerization of SA, a batch miniemulsion polymerization (Latex SA100) was carried out in a commercial calorimetric reactor (RC1, Mettler-Toledo). This reactor was equipped with a 1.5 L stainless-steel jacket reactor vessel, a fluid foil impeller, platinum resistance thermometer, electrical calibration heater, a nitrogen inlet and a sampling tube. The reactions were performed in batch at 70°C with a stirring rate of 200 rpm. The heat of reaction was estimated by assuming that total conversion was reached when the heat generation rate became zero. This assumption was checked by infrared spectroscopy (no presence of double bonds was detected). Latex 2 was synthesized using the formulation given in Table 3. The miniemulsion of SA was placed in the

Table 4. Formulations Used to Synthesize Latexes SA80 through SA20

	Latex SA80	Latex SA60	Latex SA40	Latex SA20
water	52.9	54.03	51.23	52.54
2-ethylhexyl acrylate (2EHA)	9.71	19.17	28.6	38.07
methacrylic acid (MAA)	0.27	0.45	0.61	0.79
stearyl acrylate (SA)	39.45	30.21	20.83	11.4
Dowfax 2A-1	1.17	1.14	1.21	1.1
$(NH_4)_2S_2O_8$	0.25	0.25	0.25	0.25

reactor and once the desired temperature (70 °C) was reached the initiator was added. When the conversion of SA (as monitored in the calorimeter) was 60 wt %, the 2EHA and the MAA were added as a shot.

Latexes SA80 through SA20 were obtained in batch miniemulsion polymerizations using the formulations given in Table 4. Bottles (125 mL) immersed in a thermostatic bath were used. Once the miniemulsions and the initiator system were introduced into the bottles, the bottles were purged with nitrogen for about 5 min and then tumbled end-over-end at 49 rpm in a thermostatic bath at 70 °C for 24 h.

Particle Size Distribution. Particle size distribution was determined by capillary hydrodynamic fractionation (CHDF-Matec Applied Sciences, Model 2000). The equipment was operated at 35 °C using a flow rate of 1.4 mL/min of carrier fluid (1/4X) and the detector wavelength was set at 200 nm. The sample concentration employed was less than 0.5 wt %.

Gel Fraction. The gel fraction and the swelling degree were determined by soxhlet extraction. The process consisted of a 24-hour continuous extraction with THF under reflux. After the extraction, the samples were dried and the gel content was calculated as the ratio between the non-extracted dry polymer and the initial amount of dry polymer. The swelling degree was calculated as the ratio between the weight of the swollen gel after 24 hours extraction and the weight of the dry gel.

Sol Molecular Weights. The sol molecular weights were determined by size exclusion chromatography (SEC, Waters). The setting consisted of a pump, a differential refractometer (Waters 2410) and three columns in series (Styragel HR2, HR4 and HR6; with a pore size from 1×10^2 to 1×10^6 Å). The analyses were performed at 35 °C and THF was used as solvent at a flow rate of 1 mL/min. The solution of sol polymer in THF recovered from the soxhlet extraction was dried in a ventilated oven. The dried polymer was redissolved in THF. Afterwards, it was filtered (polyamide filter $\Phi = 0.45$ μm) and the sample was injected into the SEC.

Adhesion Properties. The adhesive films used in the tests were formed under standard conditions ($T = 23$ °C and relative humidity = 55%) by spreading the latex over a flame-treated polypropylene sheet (29 μm thick) using a multiple gap applicator with reservoir. The gap was 120 μm. A 1 wt % solution of a superspreader (Silwet L-77) was previously added to the latex to improve wetting and consequently film quality. The films were dried at room temperature for 20 min. Afterwards, they were placed in a well ventilated oven at 60 °C for 10 min to evaporate completely the water. Finally, they were allowed to cool to room temperature for 10 min before being cut to make "tape strips" with the desired dimensions for each test.

Peel resistance was determined by means of the T-peel test (25). In this test, a tape strip (4 cm × 2.5 cm) was applied to the polypropylene substrate using a given pressure (2 kg roller) to make the contact. The tape's free end was clamped to the upper jaw of an Instron tensile tester, which pulled the tape at an angle of 90° at a constant speed of 300 mm/min. The average force required to peel away the tape was recorded. Shear resistance was assessed by the holding power shear test (26, 27). This test consisted of applying a standard area of tape (2.5 cm × 2.5 cm) on a polypropylene substrate under a load of 1 kg. The time to failure was recorded. The experiments were performed under different ambient temperatures using SAFT equipment (Sneep Industries).

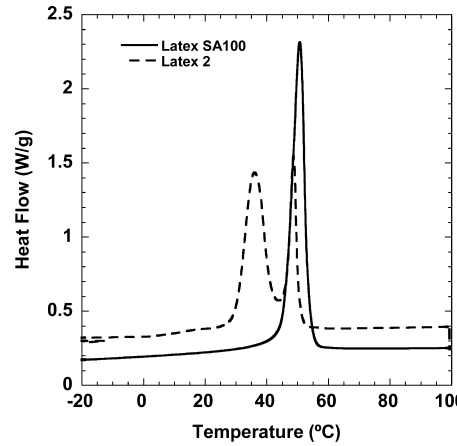

FIGURE 1. DSC thermograms of Latexes 2 and SA100.

Atomic Force Microscopy. Atomic force microscopy (AFM) measurements were performed using a commercial instrument (NTEGRA, NT-MDT, Moscow, Russia) in intermittent contact ("tapping") mode. A silicon cantilever (ATEC-NC, Nanosensors, Switzerland) with ultrasharp tip (radius of curvature less than 10 nm) was used. The nominal resonant frequency, f_0, of the cantilever was about 330 kHz and its spring constant, k, was about 45 N/m. The "free" amplitude (A_0, corresponding to oscillation in air) was fixed between 232−280 nm and the set point amplitude A_{sp} (corresponding to the amplitude when the tip is in contact with the sample surface) was kept between 104 and 130 nm. Films were cast with a 40 μm hand-held K-bar coater on a PET substrate and allowed to dry overnight at room temperature.

Differential Scanning Calorimetry. The melting temperatures of the films prepared for the adhesive tests were determined using a commercial differential scanning calorimeter, DSC (Q1000, TA Instruments). The scanning cycles consisted of first cooling to −50 °C at 10 °C/min, then heating from −50 to 100 °C at 10 °C/min, cooling again from 100 to −50 °C at 10 °C/min, and then heating to 100 °C at a rate of 10 °C/min. The results from the first heating run from −50 to 100 °C will be presented herein. The relative crystallinity degrees, X_c, of the polymers were calculated as $\Delta H_{Tot}/\Delta H_0$, where ΔH_{Tot} is the endothermic heat flow of the initially existing crystals and ΔH_0 is the endothermic heat flow of Latex SA100. ΔH_0 (28, 29) is frequently referred to as the heat flow of 100% crystalline polymer, but here the value is the approximation of a semicrystalline polymer as a 100% crystalline polymer, because there is no way of synthesising a 100% crystalline polymer. Therefore, the use of the endothermic heating of Latex SA100 was used in this work to represent the maximum obtainable crystallinity degree of poly(octadecyl acrylate) synthesized under these conditions.

RESULTS AND DISCUSSION

Figure 1 presents the DSC thermogram of Latexes 2 and SA100. It can be seen that the thermogram of Latex SA100 presents a single endotherm peak around 48 °C, which is associated with the crystals arising from the crystallization of the long alkyl chains of the stearyl acrylate. In the thermogram of Latex 2, two peaks appeared: one at about 48°C, corresponding to pure poly(stearyl acrylate), and another below 36 °C, which corresponded to the SA-rich fraction of the SA-2EHA copolymer.

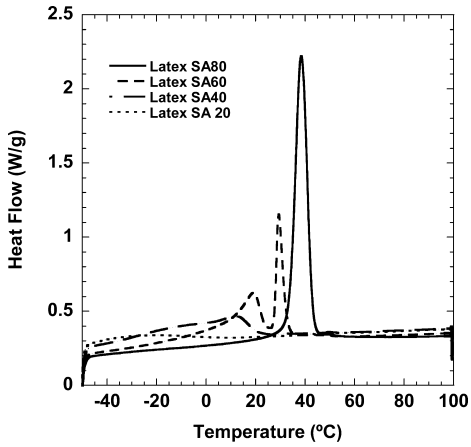

FIGURE 2. DSC thermograms of Latexes SA80–SA20.

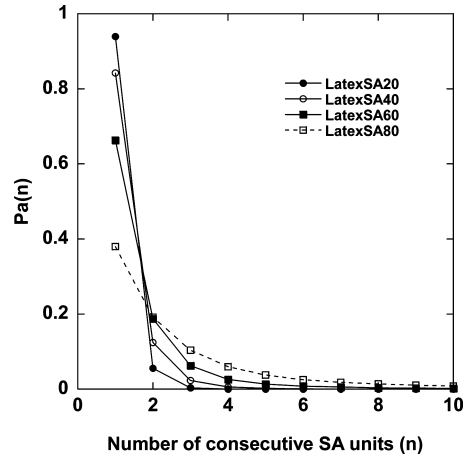

FIGURE 3. Effect of the monomer ratio in the formulation on the number monomer sequence distribution in the copolymer chains.

Figure 2 presents the DSC thermograms of Latexes SA80 through SA20. It can be seen that Latex SA80, which had the same overall formulation as Latex 2, presents a strong peak at about 35 °C but does not show the characteristic peak of poly(SA) at around 49 °C. The peak shifted to lower temperatures as the concentration of SA decreased and practically disappeared for SA concentrations lower than 40–50%.

The likely reason is that in the synthesis of Latex SA80, SA was polymerized in the presence of 2EHA and hence the sequence of contiguous SA units in the chain was disrupted by 2EHA units. To check this point, the sequence distribution of SA in the polymer chains was calculated, as it is shown in Appendix I. Figure 3 presents the predicted effect of the monomer ratio in the formulation on the monomer sequence distribution in the copolymer chains at the end of the polymerization. It can be seen that for concentration of SA lower than 50%, the fraction of long sequences of SA over the total amount of SA was negligible, which agrees with the absence of the characteristic peak of poly(SA) at about 49 °C. On the other hand, the average length of the SA sequences decreased as the SA concentration in the formulation decreased, which agrees with the lower intensity and the shift to lower temperatures of the crystalline peak.

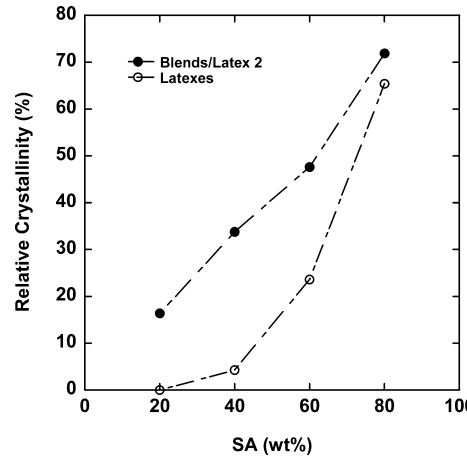

FIGURE 4. Effect of the SA concentration on the relative crystallinity degree, X_c, of Latex 2 and Blends SA60–SA20 in comparison to Latexes SA80–SA20.

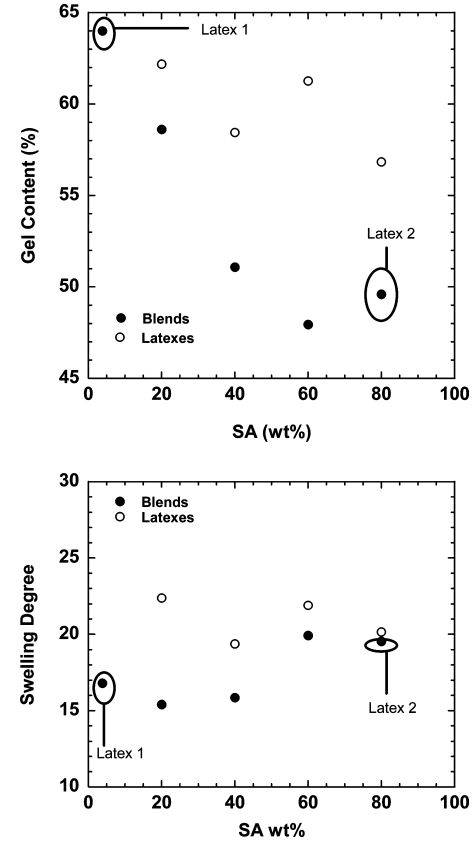

FIGURE 5. Gel content and swelling degree of the copolymer latexes and the blends.

Figure 4 presents the relative crystallinity of Latex 2 and Blends SA20 through SA60 and Latexes SA20 through SA80 as a function of the SA concentration. It can be seen that in both series the relative crystallinity increases with the SA concentration. The increase of the relative crystallinity for the blends was almost linear with respect to the SA concentration. Below 40 wt % SA, the crystallinity present in the latexes was almost negligible, but above that concentration, the crystallinity strongly increased with the SA concentration. The maximum relative crystallinity obtained for blends and latexes was similar.

Table 5. Average Molecular Weights for Latexes SA80−SA20 and Blends SA60−SA20

sample	$\bar{M}_n$	$\bar{M}_w$	D
Latex SA80	184 478	772 570	4.2
Latex SA60	155 033	682 602	4.4
Latex SA40	182 289	726 335	4.0
Latex SA20	155 912	565 206	3.6
Latex 2	129 138	839 894	6.5
Blend SA60	132 859	722 186	5.4
Blend SA40	154 170	933 580	6.1
Blend SA20	165 560	611 665	3.7
Latex 1	289 800	900 775	3.1

Adhesion properties depend on the polymer architecture (9, 30−32). In this work, the polymer architecture was characterized in terms of the gel fraction, the swelling ratio (which gives an indication of the crosslinking density in the gel) and the sol molecular weights. Figure 5 presents the values of the gel contents and swelling degrees of Latexes SA20 through SA80 in comparison to those of the blends of the Latexes 1 and 2. It can be seen that, for the same overall composition, the gel contents of Latexes SA20-SA80 were higher than those of the blends. The evolution of the gel content of the blends followed a mixing rule, and it was lower than that of the latexes because of the low gel content of Latex 2. On the other hand, the blends presented a lower swelling than the latexes because to the combined effect of the low swelling of the highly crosslinked Latex 1 and the low swelling of the crystalline Latex 2.

The number and weight-average molecular weights and the dispersities for Latexes SA20-SA80 and for the blends are presented in Table 5. It can be observed that neither the blends nor the copolymers presented significant differences. However, the blends presented broader molecular weight distributions with respect to the latexes.

The films cast from these latexes show distinctive microstructural features. The AFM image in Figure 6 shows that Latex 1 yielded a rather uniform film, showing a high level of particle deformation and coalescence of the particles, whereas Latex 2 yielded a film in which the particle identities remained, and there was less coalescence. Latex SA80, which had the same overall composition as Latex 2, but a narrower composition distribution, likewise presented individual particles at the surface of the film.

Figure 7 compares the AFM phase images of the surface of the films cast from Latexes SA60 through SA20 with those of the blends of the corresponding overall monomer compositions (Blends SA60-SA20). In these phase images, domains that dissipate less energy, when the tip interacts with it, appear brighter (33). Domains that dissipate more energy, such as materials that have a greater viscous component in their viscoelasticity (34, 35), appear darker in the AFM phase images. It can be seen that the films cast with Latexes SA60, SA40 and SA20 have a more homogeneous surface in comparison to those obtained from blends, in accordance with their more homogeneous distribution of phases. Among the copolymers in Figure 7, Latex SA60 contains the highest amount of SA. The harder domains (appearing bright in the images) can be explained as particles with a higher proportion of poly(SA). They have higher crystallinity and hence

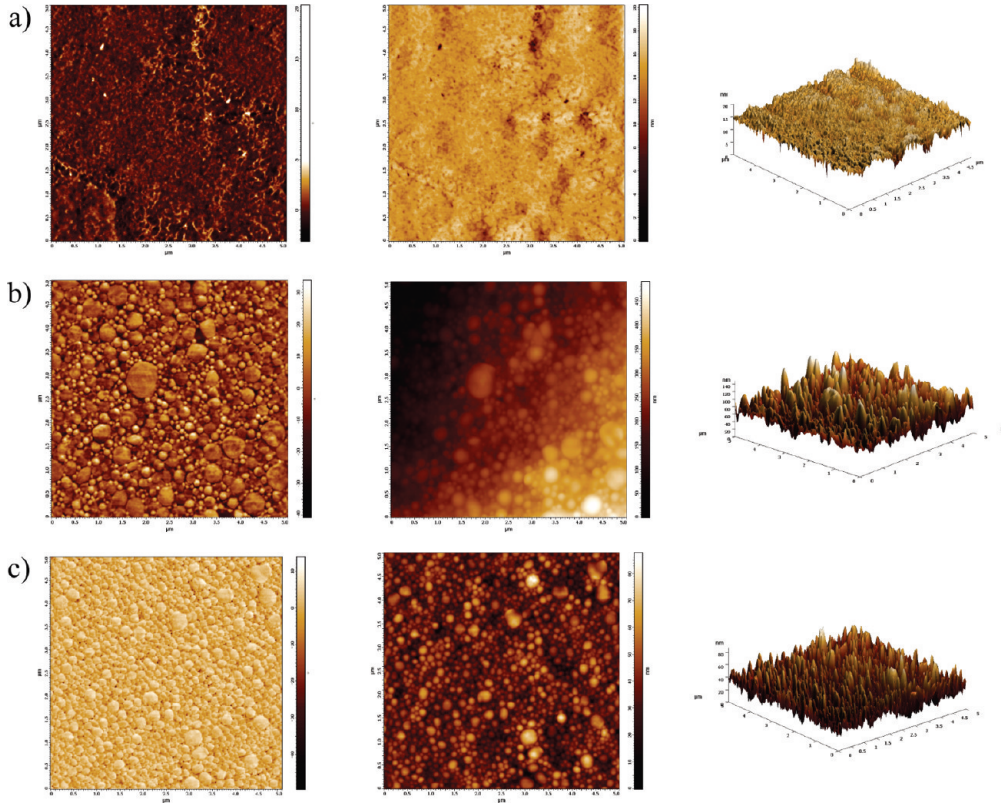

FIGURE 6. AFM phase (on the left side), height and 3D height images (on the right side) of the surface of the films cast from (a) Latex 1, (b) Latex 2, and (c) SA80. All of the images are 5 μm × 5 μm. The vertical scales for the 3D images are (a) 0−20 nm, (b) 0−140 nm, and (c) 0−80 nm.

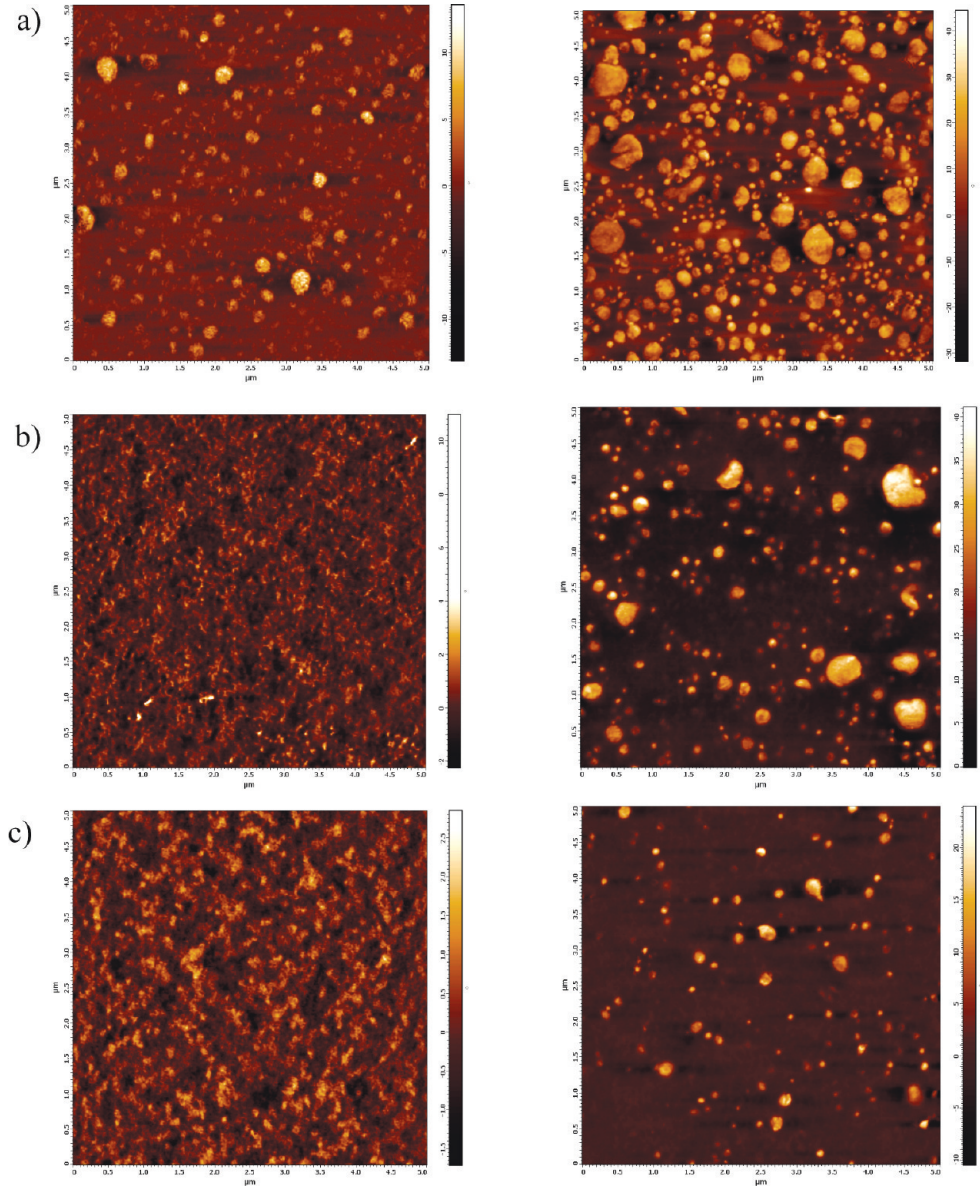

FIGURE 7. AFM phase images of latexes (on the left side) and their equivalent blends (on the right side): (a) Latex SA 60 and Blend SA 60, (b) Latex SA 40 and Blend SA 40, (c) Latex SA 20 and Blend SA 20. All images are 5 μm $\times$ 5 μm.

are denser and less viscoelastic. On the other hand, Latexes SA40 and SA20 presented a smooth film without the presence of hard domains, which is consistent with the previous interpretation of less crystallinity observed in the DSC thermograms in Figure 2.

The films cast from blends presented a continuous soft matrix in which the harder, crystalline particles were dispersed. The fraction of hard particles increased with the concentration of Latex 2, but it is interesting to notice that the area of the continuous matrix was larger than the fraction of Latex 1 used in the blends. This suggests that the surface might not be representative of the bulk of the film.

Figure 8 presents the shear resistance measured on polypropylene at 30 °C for Latexes SA60-SA20 and Blends SA60-SA20. It can be seen that the shear resistances of the blends were substantially higher than the values from the more homogeneous copolymers (Latexes SA60-SA20). On the other hand, the shear resistance of the blends increased

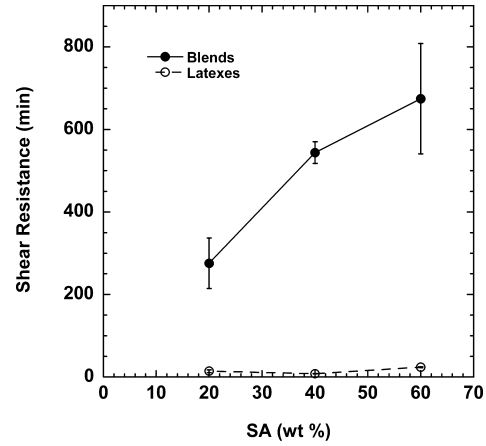

FIGURE 8. Effect of the SA concentration on shear resistance for latex blends compared to copolymer latexes.

with the content of Latex 2 and hence with increasing crystalline fraction and decreasing gel content. The latter

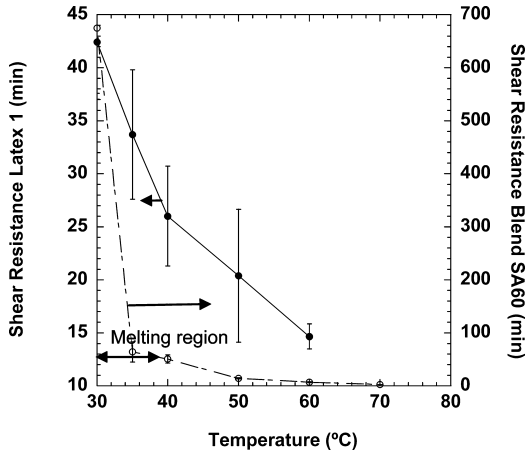

FIGURE 9. Effect of the test temperature on the shear resistance of Blend SA60 and Latex 1.

effect is interesting because the shear resistance usually increases with gel content (9, 36). This result suggests that the effect of the crystalline fraction was able to overcome the effect of the gel content. The presence of a greater crystalline fraction presumably made the material more solidlike and increased its creep resistance.

The effect of temperature on shear resistance is illustrated in Figure 9 for Blend SA60. The effect of temperature on the shear resistance of a standard PSA (Latex 1) is presented for a comparison. For this standard PSA, increasing the temperature led to a decrease in shear resistance because of the greater viscous component, resulting in a less cohesive material. It can be observed in Figure 9 that the shear resistance of Latex 1 decreased by one-third with a nearly monotonic dependence on temperature over the range from 30 to 60 °C Interestingly, the temperature dependence of shear resistance in Blend SA60 was much more abrupt. In this case, the shear resistance was reduced a factor of about 10 times by increasing the temperature from 30 to 35 °C. A further increase of the temperature led to only a moderate reduction of the shear resistance. Most likely, the dramatic decrease of the shear resistance when the temperature increased above 30 °C is due to the melting of the poly(SA) crystals. The sensitivity of the adhesion of Blend SA60 to temperature, with a large change over a narrow temperature range, opens the possibility to design temperature-responsive adhesives, in particular PSAs that strongly adhere to substrates but that can easily and abruptly removed by moderate heating.

Figure 10 presents the results of the T-peel tests for Latexes SA60-SA20 and the corresponding Blends SA60-SA20; Latex 1 is also included. Similar to what was found for the shear resistance, the blends presented significantly higher peel strengths than the copolymer latexes. As a way to show any correlation between the shear resistance and peel strength, these properties are plotted against each other in Figure 11 for all of the materials. The trend shows that Blends SA40 and SA20 showed higher peel strengths in combination with higher shear strengths, in comparison to all others, including the standard amorphous acrylate (Latex 1). This is remarkable because adhesives showing a high

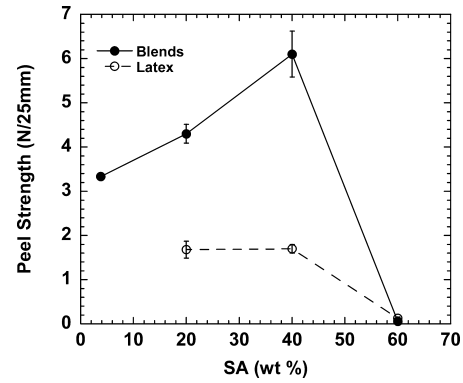

FIGURE 10. Peel strength for Latexes SA60–SA20 and Blends SA60–SA20.

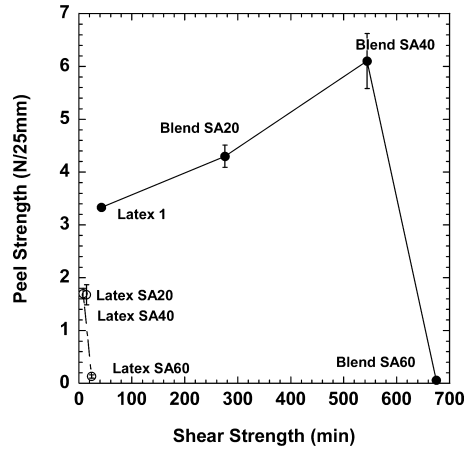

FIGURE 11. Inter-relationship of peel strength and shear resistance for Latexes SA60–SA20, Blends SA60–SA20, and Latex 1.

shear resistance usually exhibit a low peel strength (37). Whereas a high shear resistance requires a solid-like response (high creep resistance), a high peel strength requires polymer flow and associated energy dissipation, which is the response of highly viscous liquid (31, 32). These two requirements are contradictory, but nevertheless they can be met in these semicrystalline PSAs. It is worth pointing out that these latexes had similar sol molecular weights (Table 5), therefore the better performance of the blends was due to their crystalline content, which was able to overcome the counter-acting effect of the lower gel fraction. Blend SA40 (50 % of Latex 2 and 50 % of Latex 1) presents a particularly nice compromise in the optimization of both shear resistance and peel strength.

CONCLUSIONS

Semicrystalline, waterborne pressure sensitive adhesives have been synthesized and found to possess a desirable combination of properties. The crystalline fraction of the polymer was produced in situ by miniemulsion polymerization of stearyl acrylate. The degree of crystallinity was controlled by copolymerization with 2-ethylhexyl acrylate. The polymer architecture was determined by the monomer ratio in the formulation and by the process conditions.

For a given SA/2EHA monomer ratio, the maximum degree of crystallinity is achieved when all of SA is polymerized first and the 2EHA is polymerized afterwards. Because

this strategy is likely to result in phase separation between the poly(SA) and the poly(2EHA), a certain amount of poly(SA-co-2EHA) was produced to reduce phase separation. In this work, the complex latex poly(SA)/poly(SA-co-2EHA)/poly(2EHA) was mimicked by blending in different proportions of a latex that was mainly constituted of 2EHA with a semicrystalline poly(SA)/poly(SA-co-2EHA) latex. Latexes of the same overall composition but with much lower crystallinity were synthesized by copolymerizing SA and 2-EHA.

It was found that the shear resistance increased with the degree of crystallinity, which was able to overcome the effect of the decreasing gel fraction. For blends, the peel strength presented a maximum for an intermediate value of the crystallinity. Interestingly, for a given overall composition, both shear resistance and peel strength increased with the presence of a crystalline phase. This is an unusual but a valuable combination. The PSA properties were highly sensitive to temperature in the range around the crystal melting temperature, showing a high shear strength just below the melting point and a much lower value just above it. This characteristic opens up the possibility of designing temperature responsive adhesives.

Acknowledgment. The authors acknowledge the financial support provided by Diputación Foral de Guipuzkoa, Gobierno Vasco (GIC07/16-IT-303-07), the Ministerio de Educación y Ciencia (MEC CTQ 2006-03412), and an Overseas Student Scholarship at the University of Surrey. Mrs. Violeta Doukova (University of Surrey) is thanked for providing technical support for the thermal analysis.

APPENDIX I

In a batch copolymerization, the overall conversion (X_T) and the cumulative copolymer composition (B_A) are given by

$$X_T = \frac{(A_0 - A) + (B_0 - B)}{(A_0 + B_0)} \tag{I-1}$$

$$\beta_A = \frac{(A_0 - A)}{(A_0 + B_0) + (B_0 - B)} \tag{I-2}$$

where A_0 and B_0 are the initial molar amounts of monomers A and B, and A and B the molar amounts at a given time.

Let ρ_A be the product of the cumulative composition and the overall conversion

$$\rho_A = \beta_A X_T \tag{I-3}$$

The evolution of ρ_A during the batch polymerization is given by (38)

$$\frac{d\rho_A}{dX_T} = \frac{r_A\frac{A}{B} + 1}{2 + r_A\frac{A}{B} + r_B\frac{B}{A}} \tag{I-4}$$

Combination of eqs I-1, I-2, and I-3 yields

$$\frac{A}{B} = \frac{\frac{A_0}{(A_0 + B_0)} - \rho_A}{\frac{B_0}{(A_0 + B_0)} + (\rho_A - X_T)} \tag{I-5}$$

The number instantaneous monomer sequence distribution is

$$p_{AN} = p_{AA}^{n-1}(1 - p_{AA}) \tag{I-6}$$

where p_{An} is the fraction of subchains of n units of monomer A in the copolymer and p_{AA} is the probability of adding an A unit to a chain with terminal A and is given by

$$p_{AA} = \frac{1}{1 + \frac{(B/A)}{r_A}} \tag{I-7}$$

The number cumulative monomer sequence distribution is (39)

$$\overline{p_{An}} = \frac{1}{X_T}\int_0^{X_T} p_{An}\,dX_T \tag{I-8}$$

Differentiation of eq I-8 gives

$$\frac{\overline{dp_{An}}}{dX_T} = \frac{p_{An} - \overline{p_{An}}}{X_T} \tag{I-9}$$

Integration of eqs I-4 and I-9 allows the prediction of the number cumulative monomer sequence distribution.

The weight cumulative monomer sequence distribution is

$$\overline{p_{An}^W} = \frac{n\overline{p_{An}}}{\sum_{n=1}^{\infty} n\overline{p_{An}}} \tag{I-10}$$

The values of the reactivity ratios were calculated from the Q−e Scheme (40) to be

$$r_{SA} = r_A = 0.25 \tag{I-11}$$

$$r_{2EHA} = r_B = 1.43 \tag{I-12}$$

REFERENCES AND NOTES

(1) Mallégol, J.; Bennett, G.; McDonald, P. J.; Keddie, J. L.; Dupont, O. *J. Adhes.* **2006**, *82*, 217–238.
(2) Wang, T.; Lei, C.-H.; Dalton, A. B.; Creton, C.; Lin, Y.; Sun, Y.-P.; Fernando, K. A. S.; Manea, M.; Asua, J. M.; Keddie, J. L. *Adv. Mater.* **2006**, *18*, 2730–2734.

(3) Do Amaral, M.; Roos, A.; Asua, J. M.; Creton, C. *J. Colloid Inter. Sci.* **2005**, *281*, 325–338.
(4) Singa, D.; Tobing, A. K. *J. Appl. Polym. Sci.* **2001**, *79*, 2230–2244.
(5) Plessis, C.; Arzamendi, G.; Alberdi, J. M.; Angley, M.; Leiza, J. R.; Asua, J. M. *Macromolecules* **2001**, *34* (17), 6138.
(6) Crosby, A. J.; Shull, K. R. *J. Polym. Sci. Polym. Phys.* **1999**, *37*, 3455–3472.
(7) Gilbert, F. X.; Allal, A.; Marin, G.; Derail, C. *J. Adhes. Sci. Technol.* **1999**, *13* (9), 1029–1044.
(8) Toyama, M.; Ito, T.; Nukatsuka, H. *J. Appl. Polym. Sci.* **1973**, *17*, 3495–3502.
(9) Chauvet, J.; Leiza, J. R.; Asua, J. M. *Polymer* **2005**, *46*, 9555–9561.
(10) Park, Y.-J.; Kim, H.-J. *Int. J. Adhes. Adhes.* **2003**, *23*, 383–392.
(11) Sánchez-Adsuar, M. S. *Int. J. Adhes. Adhes.* **2000**, *20*, 291–298.
(12) Laurens, C.; Ober, R.; Creton, C.; Léger, L. *Macromolecules* **2001**, *34*, 2932–2936.
(13) Laurens, C.; Ober, R.; Creton, C.; Léger, L. *Macromolecules* **2004**, *37*, 6806–6813.
(14) De Crevoisier, G.; Fabre, P.; Compart, J. M.; Leibler, L. *Science* **1999**, *285*, 1246.
(15) Clarke, R.; Larson, A.; Scmitt, E. E.; Bitler, S. P. *Adhes. Age* **1993**, *39*, 41.
(16) Chivers, R. A. *Int. J. Adhes. Adhes.* **2001**, *21*, 381–88.
(17) Jordan, E. F.; Artymyshyn, B.; Specca, A.; Wrigley, A. N. *J. Polym. Sci., A* **1971**, *9*, 3339–3365.
(18) Jordan, E. F.; Feldeisen, D. W.; Wrigley, A. N. *J. Polym. Sci., A* **1971**, *9*, 3367–3378.
(19) O'Leary, K. A.; Paul, D. R. *Polymer* **2006**, *47*, 1245–1258.
(20) Lau, W. U.S. 5 521 266, 1996.
(21) Reinhold, J. L.; Walker, M. *Macromol. Chem. Phys.* **2002**, *201* (12), 1235–1243.
(22) Ugelstad, J.; El-Aaser, M. S.; Vanderhoff, J. W. *J. Polym. Sci., Polym. Lett.* **1973**, *11* (8), 503–513.
(23) Asua, J. M. *Prog. Polym. Sci* **2002**, *27*, 1283–1346.
(24) Guigliotta, L. M.; Arotcarena, M.; Leiza, J. R.; Asua, J. M. *Polymer* **1995**, *36*, 2019–1023.
(25) ASTM D 1876-95, standard test method for peel resistance of adhesives. In *Annual Book of ASTM Standards*; American Society for Testing and Materials: West Conshohocken, PA, 1996; Vol. 15.06, pp 115—117.
(26) *PSTC-7M, holding power of pressure sensitive tapes*; American Pressure Sensitive Tape Council: Naperville, IL, 1986.
(27) ASTM:D3654/D3654M-2, standard test methods for shear adhesion of pressure sensitive tapes. In *Annual Book of ASTM Standards*; American Society for Testing and Materials: West Conshohocken, PA, 1999; Vol. 15.10.
(28) Jordan, E. F.; Feldeisen, D. W.; Wrigley, A. N. *J. Polym. Sci., A* **1971**, *9*, 1835–1852.
(29) Wang, T.; Liu, D.; Keddie, J. L. *J. Appl. Polym. Sci.* **2007**, *106*, 386–393.
(30) Asua, J. M. *J. Polym. Sci., Part A: Polym. Chem.* **2004**, *42*, 1025–1041.
(31) Lindner, A.; Lestriez, B.; Marriot, S.; Creton, C.; Maevis, T.; Lütimann, B.; Brummer, R. *J. Adhes.* **2006**, *82*, 267–310.
(32) Deplace, F.; Carelli, C.; Mariot, S.; Retsos, H. Chateauminois; Ouzineb, K.; Creton, C. *J. Adhes.* **2009**, *85*, 18–54.
(33) Lei, C.; Ouzineb, K.; Dupont, O.; Keddie, J. L. *J. Colloid Interface Sci.* **2007**, *307*, 56–63.
(34) Anczykowski, B.; Gotsmann, B.; Fuchs, H.; Cleveland, J. P.; Elings, V. B. *Appl. Surf. Sci.* **1999**, *140*, 376–382.
(35) Scott, W. W.; Bhushan, B. *Ultramicroscopy* **2003**, *97*, 151.
(36) Satas, D. In *Handbook of Pressure Sensitive Adhesives Technology*, 2nd ed.; Van Nostrand Reinhold: New York, 1989.
(37) Czech, Z. *Polym. Int.* **2003**, *52*, 347–357.
(38) de la Cal, J. C.; Leiza, J. R.; Asua, J. M. *J. Polym. Sci., Part A: Polym. Chem.* **1991**, *29*, 155–167.
(39) Forcada, J.; Asua, J. M. *J. Polym. Sci., Polym. Chem. Ed.* **1985**, *23*, 1955–1962.
(40) Brandrup, A.; Immergut, E. H. In *Polymer Handbook*, 3rd ed.; Wiley Interscience: New York, 1989.

AM9006947